New Feigenbaum constants for four-dimensional volume-preserving symmetric maps

Jian-min Mao
Center for Studies of Nonlinear Dynamics, La Jolla Institute, 10280 N. Torry Pines Road, Suite 260, La Jolla, California 92037

Robert H. G. Helleman
Center for Studies of Nonlinear Dynamics, La Jolla Institute, 10280 N. Torry Pines Road, Suite 260, La Jolla, California 92037
and Department of Physics, University of Houston, University Park, Houston, Texas 77004

(Received 28 July 1986)

We study period doubling in a *symmetric* four-dimensional volume-preserving quadratic map, i.e., two *symmetrically* coupled two-dimensional area-preserving Hénon maps. We must vary *two* parameters and thus obtain *two* Feigenbaum constants, δ_1 and δ_2. It is a very important point that for each region of stability (belonging to some period-q orbit) in this parameter plane we find *two* regions of stability for the period-$2q$ orbit, four regions for the period-$4q$ orbit, and so on. Hence we have an infinite number of stability regions and infinities of bifurcation "paths" through these regions. Almost all self-similar bifurcation paths fall into one of *three* possible "universality classes," i.e., each class is characterized by its own two Feigenbaum constants, δ_1 and δ_2. We find $\delta_2=+4.000\ldots,-2.000\ldots,-4.404\ldots$, respectively, for the three classes. These δ_2 values are also recovered here from some approximate (numerical) renormalization scheme. The δ_1 is, in all cases, the same as in two-dimensional area-preserving maps, $\delta_1=8.721\ldots$. The $\delta_2=-15.1\ldots$, reported in an earlier paper [J. M. Mao, I. Satija, and B. Hu, Phys. Rev. A 32, 1927 (1985)], applies to only two exceptional paths.

I. INTRODUCTION

The period-doubling transition to chaos has been extensively studied for dissipative systems.[1] Most of the results on conservative systems exist only for two degrees of freedom, described by two-dimensional (2D) area-preserving maps.[1] Period doubling for conservative systems with three degrees of freedom, described by *four*-dimensional (4D) volume-preserving maps, has been studied more and more in recent years.[2–7] Clear evidence for an infinite period-doubling sequence in a 4D "symplectic" map has been reported[6,7] (a symplectic map is a volume-preserving map corresponding to a Hamiltonian system).[8] That infinite period-doubling sequence was determined by following a special bifurcation path in the parameter plane (the map has two parameters). Here we find many additional bifurcation paths and determine their scaling properties.

We investigate a 4D volume-preserving map which consists of two coupled 2D area-preserving maps,

$$\begin{aligned} x' &= -y + f(x,u)\ , \\ y' &= x\ , \\ u' &= -v + f(u,x)\ , \\ v' &= u\ , \end{aligned} \tag{1.1}$$

where we twice use the same quadratic function $f(x,u)$, with only its two arguments interchanged, i.e., this is a "symmetric" 4D map. This symmetry of the map simplifies calculating the periodic orbits and has other advantages. Note, however, that (1.1) is not the most general 4D volume-preserving map.

One type of periodic orbit of our map (1.1) is an orbit with $u_i=x_i$ and $v_i=y_i$, $i=1,2,\ldots,N$, where N is the period. This orbit is called an "in-phase" orbit. In this paper we will study the in-phase orbits only.

We must vary at least *two* parameters of $f(x,u)$ in order to find (follow) periodic orbits. The regions of stability we find for each of the in-phase period-doubling orbits are sketched in the parameter plane of Fig. 1. The region of stability for the in-phase period-1 orbit is the large parallelogram 1 in Fig. 1. Note that there are *two* parameter regions in which the period-2 orbit is stable (the orientation of the upper region is reversed, compared to that of the parallelogram), and so on. Hence, there is an *infinite bifurcation (tree) of stability regions in the parameter plane.*

A specific sequence of stability regions (with increasing

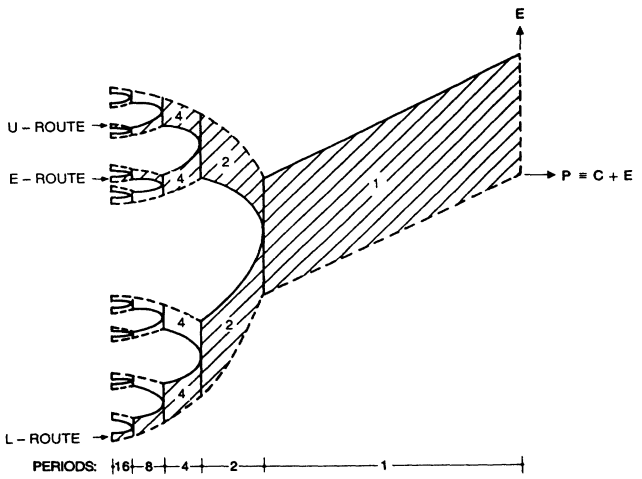

FIG. 1. A sketch of the regions of stability in the *PE*-parameter plane for the period-1, -2, -4, etc., orbits of our symmetric 4D quadratic volume-preserving map (1.1), (2.1), cf. Fig. 6. The actual regions are numerically plotted in Figs. 3–5.

period) we call a bifurcation *"route."* A specific one-dimensional parameter curve within a route we call a bifurcation *"path."* We find that all self-similar bifurcation routes can be classified into three types: L, U, or E routes. The L routes arise from always choosing the upper (or always the lower) branch of the stable region when the period doubles, whereas for the U (and E) routes the subsequent regions of stability alternate between the upper and the lower branches. A typical example of the L and U routes are indicated in Fig. 1 (there is, however, only one E route, cf. Fig. 1). "Almost all" bifurcation paths within each type of bifurcation route have the same Feigenbaum constants, δ_1 and δ_2 (the δ_1 and δ_2 are the asymptotic rates at which specific points in each region of stability converge towards a point in the parameter plane, as we go to higher and higher periods). We obtain three different values for δ_2, $+4.000\ldots$, $-2.000\ldots$, and $-4.404\ldots$, corresponding to, respectively, the L, U, and E routes. Nevertheless, in all cases, the other Feigenbaum constant δ_1 has the *same* value as in 2D area-preserving maps, $\delta_1=8.721\,09\ldots$.

Moreover, within each bifurcation route there is one *exceptional* (degenerate?), "irregular," path with a totally different δ_2. For the L and U routes this exceptional δ_2 is $-15.1\ldots$. The exceptional path in the E route has no δ_2 value at all (it runs along a parameter axis corresponding to two *un*coupled 2D maps). The exceptional $\delta_2=-15.1\ldots$ was reported earlier in Refs. 6 and 7. It may be another sign of degeneracy that this δ_2 (numerically) seems to be dependent solely on the other scaling constants of 2D area-preserving maps, i.e., $\delta_2\approx(2\alpha\beta)/\delta_1$, cf. Ref. 7.

In Sec. IV we present some approximate (numerical) renormalization. It does yield δ_2 (and δ_1) values which are very close to the actual numerical values we find for the *regular* paths. From this approximate renormalization, however, we do *not* recover the δ_2 value ($-15.1\ldots$) of the exceptional paths. The approximate renormalization scheme also gives the accumulation values for the four eigenvalues of the Jacobian matrix of the in-phase periodic orbits. These are, respectively, $(\lambda_1,1/\lambda_1,1,1)$, $(\lambda_1,1/\lambda_1,e^{i2\pi/3},e^{-i2\pi/3})$, and $(\lambda_1,1/\lambda_1,\lambda_1,1/\lambda_1)$ for the L, U, and E routes, where λ_1 ($=-2.0575\ldots$, Ref. 9) is the same as for 2D area-preserving maps. A more accurate renormalization scheme[10] confirms these results. The latter renormalization has also been extended to a class of nonsymmetric maps [i.e., Eq. (2.1) with $f\neq g$] which is much larger than the class of symmetric maps discussed here. Nevertheless, it produces the same δ_1 and δ_2 value as found here for the symmetric map.

The bifurcation tree of the stability regions will be discussed in Sec. II. The three types of bifurcation routes in the tree are identified, and the scaling for their paths is obtained in Sec. III. Numerical results of an approximate renormalization calculation are given in Sec. IV. Section V is a summary.

II. REGIONS OF STABILITY BIFURCATE IN THE PARAMETER PLANE

Consider a symmetric quadratic (volume-preserving) 4D map which consists of two coupled 2D Hénon maps:

$$\begin{aligned} x' &= -y+f(x,u)\ , \\ y' &= x\ , \\ u' &= -v+g(x,u)\ , \\ v' &= u\ , \end{aligned} \tag{2.1}$$

where

$$f(x,u)\equiv 2[(Cx+x^2)+E(u+Fu^2+Gxu)]\ , \tag{2.2}$$

$$g(x,u)\equiv f(u,x)\ . \tag{2.3}$$

Here C, E, F, and G are parameters. When the coupling parameter E vanishes, the two 2D maps uncouple. We shall often use a new parameter $P\equiv C+E$.

From the obvious period-1 orbit (fixed point) at the origin of phase space, two period-2 orbits bifurcate. Here we shall always consider only one of those two, the *in-phase* orbit (to follow the jargon of Ref. 11 for coupled logistic maps),

$$\begin{bmatrix} u_i \\ v_i \end{bmatrix} = \begin{bmatrix} x_i \\ y_i \end{bmatrix},\quad i=1,2,\ldots,N \tag{2.4}$$

where N is the period. (There also is an "opposite-phase" orbit, with $u_i=x_{i+N/2}$, $v_i=y_{i+N/2}$, which we do not consider here.)

The map (2.1) is *symplectic*[8] if

$$\frac{\partial f}{\partial u}=\frac{\partial g}{\partial x}\ . \tag{2.5}$$

For any 4D symplectic map, eigenvalues of the Jacobian matrix $\underline{J}$ come in pairs, and the Jacobian matrix has only two independent invariants

$$\begin{aligned} T_1 &\equiv \sum_{i=1}^{4}\lambda_i=\mathrm{Tr}\underline{J}\ , \\ T_2 &\equiv \sum_{\substack{i,j \\ (i<j)}}\lambda_i\lambda_j=\tfrac{1}{2}[(\mathrm{Tr}\underline{J})^2-\mathrm{Tr}(\underline{J}^2)]\ , \end{aligned} \tag{2.6}$$

where the λ's are the eigenvalues of $\underline{J}$. Stability regions for 4D symplectic maps in the T_1T_2 plane are sketched[2] in Fig. 2. The shaded region is stable. It is bounded by three curves: the period-doubling bifurcation (PDB) line segment AC [$T_2=-2T_1-2$ between $(0,-2)$ and $(-4,6)$], the tangent bifurcation (TB) line [$T_2=2T_1-2$ between $(0,-2)$ and $(4,6)$], and the "complex" bifurcation (CB) line (the parabola $T_2=T_1^2/4+2$).

The map (2.1) is a *volume-preserving* map, whence $\mathrm{Det}\underline{J}=1$ (symplectic only if $G=2F$). Yet, for the in-phase orbits, Eq. (2.5) is always satisfied due to the symmetry of the map, Eq. (2.3). Hence Fig. 2 also is the stability diagram for the in-phase orbits of the volume-preserving map (2.1). Transferring the stability diagram from the trace plane (T_1T_2 plane, Fig. 2) to our parameter plane (the PE plane, Fig. 3, at fixed values of F and G; remember $P\equiv C+E$) will clarify the complicated period-doubling picture.

For the obvious period-1 orbit at the origin of phase space,

$$(x,y,u,v)=(0,0,0,0)\ , \tag{2.7}$$

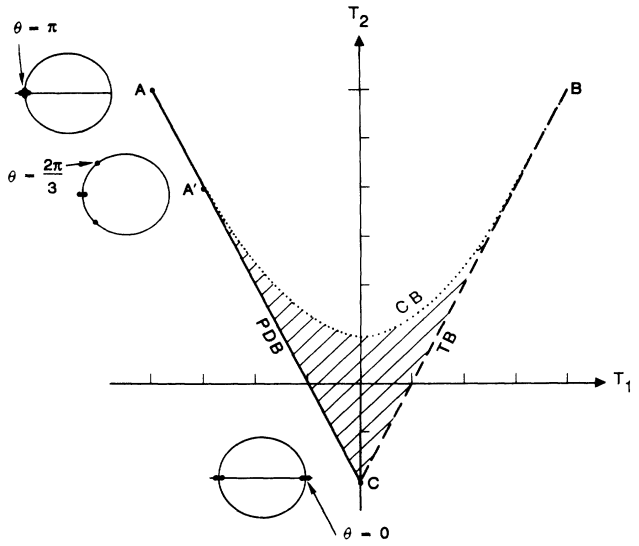

FIG. 2. Stable regions in the "trace plane" for 4D symplectic maps: the T_1 and T_2 are defined in Eq. (2.6). In all figures, the PDB line is denoted by a solid line, the TB line is denoted by a dashed line, and the CB curve is denoted by a dotted curve.

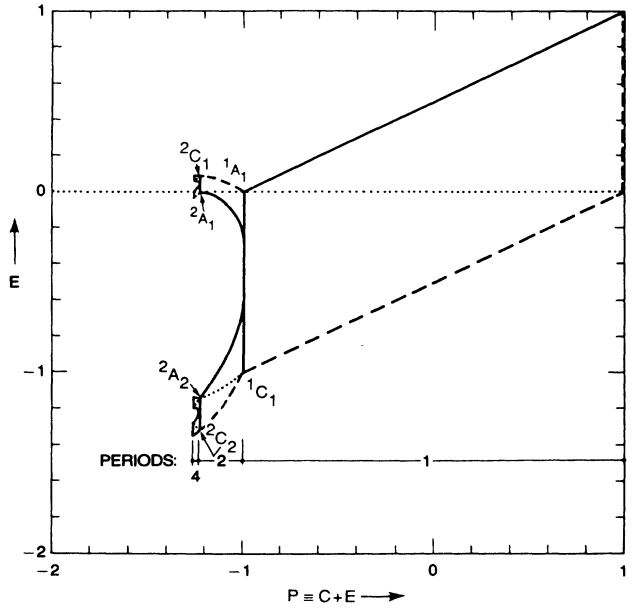

FIG. 3. Stable regions in the parameter plane for the in-phase orbits of the map (2.1) at $F=1$ and $G=2$. The stable regions are shown for the periods 1, 2, and 4. In all figures, the images of the two end points of the period-doubling bifurcation line (A and C in Fig. 2) are labeled by ${}^{N}A_i$ and ${}^{N}C_i$, where N is the period, and i denumbers the different images, $i=1,2,\ldots,N$.

we can express the PDB lines in our parameter plane (cf. Fig. 3) as $P=-1$ and $P-2E=-1$. The TB lines are $P=1$ and $P-2E=1$, and the CB curve is $E=0$. That is, the period-1 stable region is a parallelogram containing two triangles, each of which is an image of the shaded region in Fig. 2. They have a common boundary, the CB curve $E=0$.

There are *two* stable, quadrangular, regions ("branches") for the in-phase period-2 orbits, as calculated in Appendix A. Note that the orientation of the upper quadrangle is reversed, compared to that of the period-1 parallelogram. The stable regions of period 4 are also analytically given in Appendix A. These regions have four quadrangular branches. Figure 3 shows the period-1 stable region bifurcating into two period-2 stable regions, and each of those bifurcating into two period-4 stable regions, as well as those four period-4 regions, and so on. That is, each "mother" region produces two "daughter" regions when the period doubles. Since daughter regions are much smaller in size than their mother region, stable regions for very high periods will be nearly invisible. In order to, nevertheless, see some details, we replot the horizontal axis on a logarithmic scale in Fig. 4 for the upper stable regions (of Fig. 3). In Fig. 5, we even replot *both* axes logarithmically. Figure 6 is a schematic illustration of the stable region bifurcation, which will be used frequently. Figure 1 is a simplified version of Fig. 6.

In Figs. 3–6, the period-doubling bifurcation lines for different periods (such as the line ${}^{1}A_1\,{}^{1}C_1$, the lines ${}^{2}C_1\,{}^{2}A_1$, ${}^{2}A_2\,{}^{2}C_2$, etc. in Fig. 6) are parallel. Why this is so is explained in Appendix B. It is also explained there why $E=0$ is a CB curve.

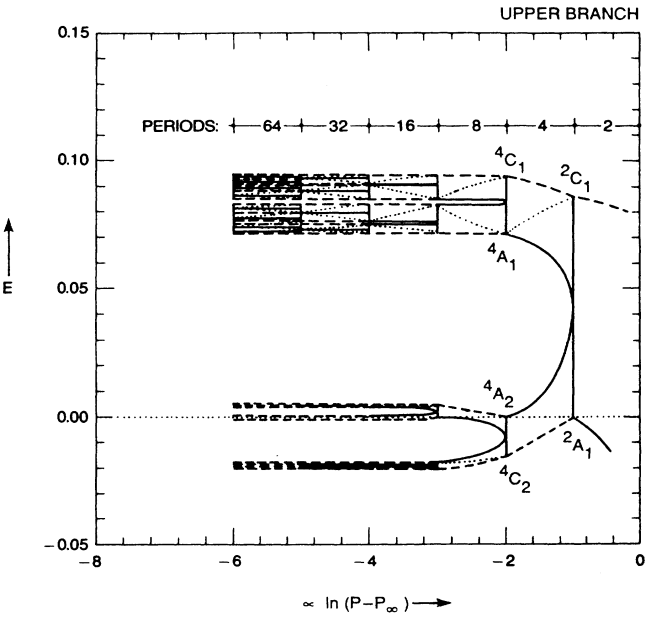

FIG. 4. Singly logarithmic plot of the stable regions of our map (2.1), at $F=1$ and $G=2$, for periods up to 64. Only the "upper" stable regions are shown. The P_∞ on the horizontal axis is the accumulation value of the parameter P, $P_\infty=-1.266\,311\,27\ldots$.

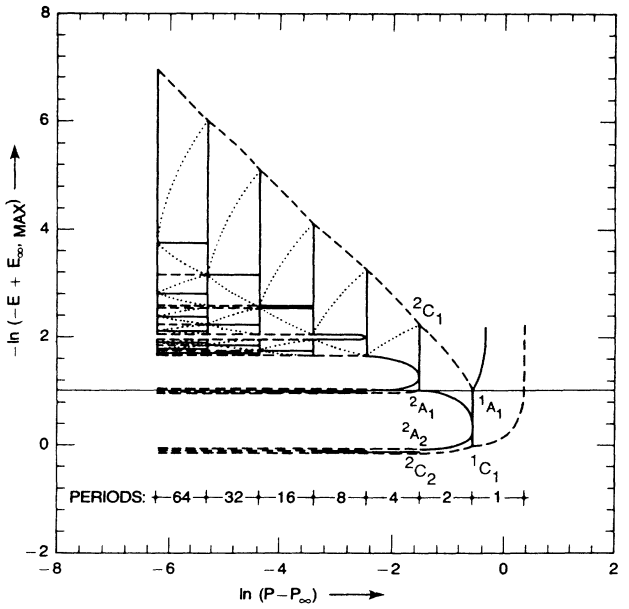

FIG. 5. Doubly logarithmic plot of the stable regions of our map (2.1), at $F=1$ and $G=2$, for periods up to 64. The $E_{\infty,\max}$ on the vertical axis is the largest of the accumulation values of E, $E_{\infty,\max}=0.094\,187\,030\,4\ldots$.

III. PERIOD-DOUBLING BIFURCATION ROUTES AND SCALING FACTORS

An enormous number of different bifurcation routes (such as the three routes in Fig. 1) follow from the previous arguments (and from Fig. 6). We will classify them into three types (the L, U, and E routes) in this section.

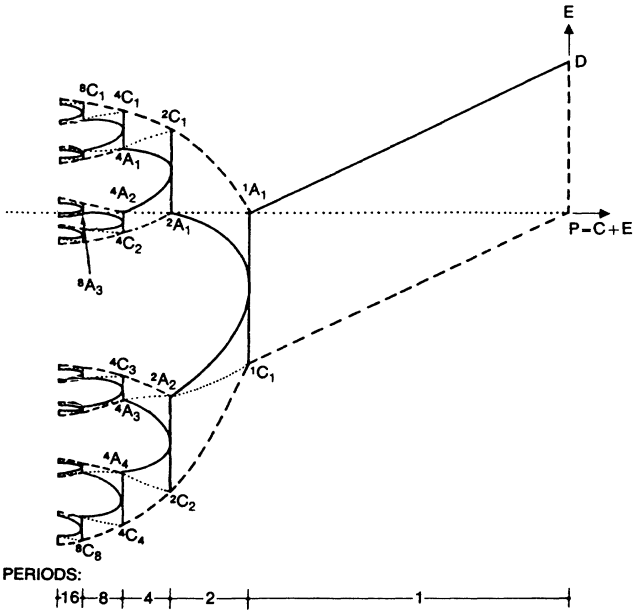

FIG. 6. Schematic illustration of the stable regions of the map (2.1) for periods up to 16, cf. Figs. 1 and 3–5.

For instance, the lowest route in Fig. 1 arises from always choosing the lower branches. It will be labeled as $(---\cdots)$ or $(-)^n$, where $-$ $(+)$ denotes choosing the lower (upper) branch. Since we are interested only in the asymptotic behavior of the period doubling, all routes labeled by $\cdots(+)^n$ or $\cdots(-)^n$ are numerically found to have a similar asymptotic behavior, and will be called L routes. That is, an L route is followed if one always chooses the upper branch at each bifurcation (or always the lower branch), from some period on.

A U route is followed if we alternate forever the upper and lower branches at consecutive bifurcations, from some period on. It will be labeled $\cdots(+\ -)^n$. The route marked U route in Fig. 1 is just an example.

One special U route is called the E route. Along it the parameter E approaches zero. It has different scaling properties from the other U routes.

Below we define bifurcation "points," "paths," and "routes."

A. Bifurcation points

We are interested only in period doublings that are asymptotically self-similar. This self-similarity requires[7] that each higher-order bifurcation should occur at the same point (the bifurcation point) on the period-doubling line segment AC in Fig. 2. Any point on AC can be a bifurcation point. Such a bifurcation point on AC corresponds to an eigenvalue configuration of the Jacobian matrix,

$$(\lambda_1,\lambda_2,\lambda_3,\lambda_4)=(-1,-1,e^{i\theta},e^{-i\theta})\ , \tag{3.1}$$

where the λ_i's are the eigenvalues, and θ is the phase angle of the second pair of eigenvalues, $0\le\theta\le\pi$. Hence, the θ specifies a bifurcation point on AC. Bifurcation points with $0\le\theta\le\pi/2$ will be called L_θ points, while points with $\pi/2<\theta\le\pi$ will be called U_θ points. The L_θ points lie on the *lower* half of AC (in Fig. 2), whereas the U_θ points lie on the *upper* half. If θ does not need to be specified, the terms "L point" and "U point" will be used.

We can always continue from one region of stability (for period 2^n) into the next region of stability (for period 2^{n+1}) at any fixed value of θ, and do so forever. The above constitutes a self-similar recipe for period doubling (remember that we have a bifurcation *line* in 4D maps, instead of a bifurcation *point* as in the 2D case, see Sec. II). In Sec. IV, we study self-similarity under a renormalization operation. Under that operation, working at a fixed value of θ does, however, not give a self-similar recipe. The only fixed θ values which yield a self-similar renormalization are $\theta=0$, $2\pi/3$, and π. For the first two values ($\theta=0,2\pi/3$), the second pair of eigenvalues in Eq. (3.1) interchanges when the period doubles. In the E route, the points with $\theta=\pi$ are special (not so in the general U routes) since the 4D map then separates into two *un*coupled 2D maps. Hence,

$$\theta=0,2\pi/3,\pi\ \ (\pi\text{: for } E=0) \tag{3.2}$$

are the most important bifurcation points in the sense mentioned above.

B. Bifurcation paths

A bifurcation point on the trace (stability) plane (Fig. 2) has N images in the PE-parameter plane (Fig. 6) for our period-N in-phase orbit. The images of the two end points (A and C) of the bifurcation line are labeled ${}^{N}A_i$ and ${}^{N}C_i$ in Figs. 3–6, where N is the period, and i denumbers the images ($i=1,2,\ldots,N$).

After the bifurcation point (specified by θ) has been chosen, its images under period doubling form a self-similar bifurcation path. For instance, if we choose the C point ($\theta=0$) as the bifurcation point, then the first period-doubling bifurcation occurs at its image ${}^{1}C_1$, and we are in the lower period-2 branch. A second bifurcation occurs at the point ${}^{2}C_2$, and so on, obtaining the bifurcation path $({}^{1}C_1,{}^{2}C_2,{}^{4}C_4,{}^{8}C_8,\ldots)$.

Furthermore, the top path in Fig. 6 $({}^{1}A_1,{}^{2}C_1,{}^{4}C_1,{}^{8}C_1,\ldots)$ is an *asymptotically* self-similar bifurcation path (here the self-similar period doubling starts at second order) also with $\theta=0$. Hence each bifurcation point (fixed θ) corresponds to an infinity of (asymptotically) self-similar bifurcation paths. A bifurcation path with $0\le\theta\le\pi/2$ will be called an L_θ path (or an L path if θ is not specified), while a path with $\pi/2<\theta\le\pi$ will be called a U_θ path (respectively, U path). In this notation, $({}^{1}C_1,{}^{2}C_2,{}^{4}C_4,{}^{8}C_8,\ldots)$ as well as $({}^{1}A_1,{}^{2}C_1,{}^{4}C_1,{}^{8}C_1,\ldots)$ are L_0 paths.

C. Bifurcation routes

Consider the lowest path $({}^{1}C_1,{}^{2}C_2,{}^{4}C_4,\ldots)$, which is an L_0 path ($\theta=0$). Gradually increasing θ by small steps, we have a set of bifurcation paths L_θ ($0<\theta<\pi/2$) in the neighborhood of this L_0 path. All those L_θ paths ($0\le\theta<\pi/2$) which can be continuously deformed into our L_0 path form the lowest *route* ("L route") in Fig. 1. Thus, an L route is a route formed by a particular L path and all L_θ paths ($0\le\theta<\pi/2$) in its neighborhood. Similarly, we define the U route as the route formed by a particular U_θ path and all U_θ paths ($\pi/2<\theta\le\pi$) in its neighborhood.

The particular U route containing the axis $E=0$ we call the "E route," as indicated in Fig. 1. For any path in this E route (called E_θ path), the coupling parameter $E\to0$ when the period increases, and the 4D map will asymptotically uncouple into two 2D maps. Numerical calculations (see Secs. III D and III E) show that this E route has a special scaling.

D. The contraction rate of the stable regions

We define the "thickness" d_n of each stable region (in a bifurcation route) as the length of the image of the period-doubling bifurcation line segment AC, cf. Figs. 2–6 (i.e., $d_n\equiv{}^{N}A_m\,{}^{N}C_m$, where $N=2^n$ is the period, m is determined by the bifurcation route). For the lowest L_0 route (see Fig. 6), $d_1={}^{1}A_1\,{}^{1}C_1$, $d_2={}^{2}A_2\,{}^{2}C_2$, ..., $d_n={}^{N}A_N\,{}^{N}C_N$, $\cdots$. This thickness vanishes geometrically at a rate

$$\gamma_n\equiv\frac{d_{n-1}}{d_n}\underset{n\to\infty}{\to}\gamma\ , \tag{3.3}$$

called the "*contraction*" rate (of the stable regions).

Numerical calculation indicates that the three types of bifurcation routes have their own contraction rates:

$$\gamma_L=4.000\ldots,\quad \gamma_U=-2.000\ldots,\quad \gamma_E=-4.404\ldots\ . \tag{3.4}$$

These values turn out to be independent of the values of the parameters F and G in the map (2.1), as shown in Table I. One might hope so as we are considering a codimension-two problem.

E. Scaling of period-doubling sequences

As an example, consider the lowest L_0 path in Fig. 6 $({}^{1}C_1,{}^{2}C_2,{}^{4}C_4,{}^{8}C_8,\ldots)$. The nth period-doubling bifurcation occurs at the point ${}^{N}C_N$, where $N=2^n$. Let P_n ($\equiv C_n+E_n$) and E_n be the coordinates of the point ${}^{N}C_N$. Scaling behavior of the period-doubling sequence $[(P_n,E_n),\ n=1,2,\ldots]$ can be determined by matrix scaling.[6] One defines a 2×2 scaling matrix $\underline{D}_n$ as follows:

$$\begin{bmatrix}P_n-P_{n-1}\\E_n-E_{n-1}\end{bmatrix}\equiv\underline{D}_n\begin{bmatrix}P_{n+1}-P_n\\E_{n+1}-E_n\end{bmatrix}\ , \tag{3.5}$$

where

$$\underline{D}_n\underset{n\to\infty}{\to}\underline{D}\ , \tag{3.6}$$

due to the self-similarity. Here $\underline{D}$ is a constant matrix. The eigenvalues of $\underline{D}$, δ_1, and δ_2, are the convergence rates of the parameters. It yields

$$\delta_1=8.721\,096\ldots \tag{3.7}$$

for all cases. This δ_1 value is the same as in the 2D area-preserving maps. The δ_2 values, however, are different for the three types of bifurcation routes (L, U, and E routes). For all L_θ paths with $0<\theta\le\pi/2$ (i.e., $\theta\neq0$) we thus find

$$\delta_2=4.000\ldots\ , \tag{3.8}$$

whereas for the exceptional L path (i.e., with $\theta=0$) we find

$$\delta_2=-15.1\ldots\quad(\theta=0)\ . \tag{3.9}$$

Similarly, all U_θ paths ($\pi/2<\theta\le\pi$, $\theta\neq2\pi/3$) have the same δ_2 value,

$$\delta_2=-2.000\ldots\ , \tag{3.10}$$

TABLE I. The contraction rate γ, Eq. (3.3), of the thickness of stable regions is given for the E route at some values of the parameters F and G. Note that γ seems to be virtually independent of F and G.

F	G	γ_E
1	2	−4.403 924 9...
2	4	−4.403 793 9...
−4	−8	−4.403 981 0...
1	3	−4.403 760 3...
1	8	−4.403 862 4...

whereas for the exceptional $U_{2\pi/3}$ path we find

$$\delta_2 = -15.1\ldots \quad (\theta = 2\pi/3) . \tag{3.11}$$

Finally, all E_θ paths with $\theta \neq \pi$ have the same δ_2 value,

$$\delta_2 = -4.404\ldots , \tag{3.12}$$

whereas no δ_2 exists for the exceptional E_π path, since all bifurcation points lie on the P axis ($E_n = 0$ for all n). We note that the δ_2's for the three types of *regular* bifurcation paths (i.e., the nonexceptional paths) equal the contraction rates γ for the same route, cf. Table II. We also note that the three types of exceptional paths correspond to the three special values of θ,

$$\theta = 0, \frac{2\pi}{3}, \pi , \tag{3.13}$$

mentioned in Eq. (3.2).

F. Orbital scaling factors

After making a linear transformation [see Eq. (A2) in Appendix A], the Jacobian matrix of the map at the in-phase orbit decomposes into two 2×2 matrices, see Eq. (A5). Hence the first two coordinates s_1 and s_2, in Eq. (A2), of the in-phase orbit (i.e., $d_1 = d_2 = 0$) are determined using the *two*-dimensional Hénon map

$$\begin{aligned} s_1' &= -s_2 + f_1(s_1, 0) , \\ s_2' &= s_1 . \end{aligned} \tag{3.14}$$

That is, the s_1 and s_2 scale with the usual 2D orbital scaling factors[1] $\alpha = -4.018\ldots$ and $\beta = 16.36\ldots$. Furthermore, according to the definition of s_1 and s_2 [i.e., Eq. (A1)], the coordinates x and y (or u and v) of the in-phase orbit also with the same scale 2D factors α and β.

IV. AN APPROXIMATE RENORMALIZATION CALCULATION

A. Eigenvalue-matching renormalization

Based on the self-similarity of period doubling, many renormalization methods have been invented.[12–14] In order to describe our present renormalization method first consider quadratic 2D area-preserving maps F_c, which can depend on one parameter only, called c. The trace t of the Jacobian matrix of a period-N orbit (i.e., of F_c^N) depends on the c and N,

$$t = t(c) . \tag{4.1}$$

All curves $t = t(c)$ for different periods in the ct plane will asymptotically intersect at a critical point (c_∞, t_∞). Consider a new map F_C^{2N}, i.e. (F_C applied $2N$ times and), at some other value, C, of the parameter c. Locally, near the period-$2N$ orbit, the new map again resembles F_c^N. This self-similarity therefore yields

$$t(c) = T(C) , \tag{4.2}$$

where t is the trace of the Jacobian matrix of the map F_c^N at its fixed point, whereas T is the trace of the Jacobian matrix of the F_C^{2N} at its new fixed point. Solving Eq. (4.2) for c gives a recursion relation for the parameter,

$$c = c(C) . \tag{4.3}$$

The critical value of the parameter is a fixed point of Eq. (4.3),[12–14]

$$C_\infty = c(C_\infty) . \tag{4.4}$$

The convergence rate of the parameters is determined by

$$\delta = \left. \frac{dc}{dC} \right|_{C_\infty} . \tag{4.5}$$

Our actual 4D map (2.1) has *two* parameters ($P \equiv C + E$ and E). Note that we fix the values of the other two parameters F and G. This 4D map has two independent invariants of the Jacobian matrix T_1 and T_2, as defined in Eq. (2.6). Hence, we work with two vectors $\mathbf{C} \equiv (P, E)$, $\mathbf{T} \equiv (T_1, T_2)$, and Eqs. (4.2)–(4.5) are used in vector-matrix forms.

B. First-order approximation

In Appendix A we apply the map twice and analytically obtain the "first-order" results (from period 1 to 2) as

TABLE II. Numerical results. The convergence rates (of the parameters) δ_1 and δ_2, Eqs. (3.6)–(3.8), and the contraction rate γ for the three types of bifurcation routes. The θ is defined in Eq. (3.1). Also note Table III.

	Route	δ_1	δ_2	γ
L route	$0 < \theta \leq \frac{\pi}{2}$		4.000...	4.000...
	$\theta = 0$		$-15.1\ldots$	
U route	$\frac{\pi}{2} < \theta \leq \pi,\ \theta \neq \frac{2\pi}{3}$	8.721 096...	$-2.000\ldots$	$-2.000\ldots$
	$\theta = \frac{2\pi}{3}$		$-15.1\ldots$	
E route	$\frac{\pi}{2} < \theta < \pi$		$-4.404\ldots$	$-4.404\ldots$
	$\theta = \pi$		nonexistent	

$$
\begin{aligned}
t_1 &= +4(p-e) , \\
t_2 &= 4(p^2-2pe)+2 , \\
T_1 &= -4(2P^2-4P-7)+16E+16E^2+8E\Phi(P,E) , \\
T_2 &= 4(2P^2-4P-7)\{(2P^2-4P-7) \\
&\qquad -4E[2+2E+\Phi(P,E)]\} ,
\end{aligned}
\tag{4.6}
$$

where $\Phi(P,E) \equiv H(P+1)(P-2E-4+2H)$, $H \equiv (2F+G)/(1+EF+EG)$, see Eq. (A11). Setting $t_1 = T_1$ and $t_2 = T_2$ in Eq. (4.6), and solving for p and e simultaneously, we obtain the recursion relations for the parameters

$$
\begin{aligned}
p &= -2P^2+4P+7 , \\
e &= -2E[2+2E+\Phi(P,E)] .
\end{aligned}
\tag{4.7}
$$

The critical fixed point values of the parameters, determined by setting $p = P = P_\infty$ and $e = E = E_\infty$ in Eq. (4.7), are $P_\infty = -1.2656\ldots$ (the same as in 2D maps) and (at most) four different solutions for E_∞, which we can solve numerically when necessary. In order to calculate the convergence rates of the parameters from Eq. (4.5), we use

$$
\underline{D} = \begin{bmatrix} \frac{\partial p}{\partial P} & \frac{\partial p}{\partial E} \\ \frac{\partial e}{\partial P} & \frac{\partial e}{\partial E} \end{bmatrix} ,
\tag{4.8}
$$

evaluated at (P_∞, E_∞). Using Eq. (4.7), we finds its eigenvalues

$$
\begin{aligned}
\delta_1 &= 4(1-P_\infty) = 9.06\ldots , \\
\delta_2 &= -4-8E_\infty+(3P_\infty+1)H_\infty\left[1-E_\infty H_\infty\frac{F+G}{2F+G}\right] \\
&\quad +4(P_\infty+1)E_\infty\left[2H_\infty(1-H_\infty)\right. \\
&\qquad \left. -E_\infty H_\infty^2(1-2H_\infty)\frac{F+G}{2F+G}\right] .
\end{aligned}
\tag{4.9}
$$

We see, however, from Eq. (4.9) that this δ_2 varies with F and G, i.e., for every new choice of F and G, we would get another δ_2 value, contrary to our numerical evidence. Hence we do not (numerically) evaluate these results (above). Instead, we numerically proceed to higher-order approximations. It turns out that the higher the order at which we start the renormalization, the less dependence there is on F and G. A more complete renormalization including renormalization equations for F and G, will be published elsewhere.

C. Renormalization at higher periods

The same renormalization calculation can numerically be done starting at higher periods (e.g., from period 2 to 4, 4 to 8, etc.). We have done this up to period 32, i.e., from the period 32 to 64. All results in this subsection are for the 32-64 renormalization (cf. Table III).

The critical value of the parameter P is the usual 2D one, $P_\infty = -1.263\,113\ldots$, and $\delta_1 = 8.721\,09\ldots$, i.e., the same as those in 2D area-preserving maps.

There might be (at most) 128 different δ_2's, corresponding to 128 different E_∞'s in this 32-64 renormalization, cf. Eq. (4.7). All δ_2 values we checked, however, are equal to one of the following three values:

$$
\delta_2 = 4.00\ldots , \quad -2.00\ldots , \quad -4.35\ldots .
\tag{4.10}
$$

Note that these renormalization values are (approximately) the same as found numerically in Eqs. (3.8), (3.10), and (3.12) for the regular paths, but do not include the $\delta_2 = -15.1\ldots$ value for the exceptional paths.

The eigenvalues of the Jacobian matrix limit on one of three eigenvalue configurations (for the three types of bifurcations routes). These configurations are listed in Table III. The first two eigenvalues are always $\lambda_1 = -2.0575\ldots$ and $1/\lambda_1$, which are the same as those[9] for 2D area-preserving maps. However, the second pair of eigenvalues for the L and U route is on the unit circle with phase angle $\theta = 0$ and $2\pi/3$, respectively, (remember that these L_0 and $U_{2\pi/3}$ paths are the exceptional L and U paths). The second pair of eigenvalues for the E route ($E_\infty = 0$, remember that the axis $E = 0$ is the exceptional path in the E route) are the same as in the 2D area-preserving map. Both numerically and in the renormalization approximation, we find that all regular paths in each route *limit* on the special path of that route. Nevertheless the numerical and renormalization values of δ_2, for the regular paths, appear *not* to limit on the δ_2

TABLE III. Some fixed-point results of the approximate renormalization calculation of Sec. IV C. The $\lambda_1, \ldots, \lambda_4$ are the eigenvalues of the Jacobian matrix. The λ_1 value is the same as in 2D maps ($\lambda_1 = -2.0575\ldots$). Note that the numerical results of Table II are recovered here (except for the exceptional paths with $\delta_2 = -15.1\ldots$) to a very good approximation.

Route	δ_1	δ_2	Eigenvalues $(\lambda_1,\lambda_2,\lambda_3,\lambda_4)$	$\lambda_3+\lambda_4$
L route	8.721...	4.00...	$\left(\lambda_1, \frac{1}{\lambda_1}, 1, 1\right)$	2.00...
U route	8.721...	−2.00...	$\left(\lambda_1, \frac{1}{\lambda_1}, e^{i2\pi/3}, e^{-i2\pi/3}\right)$	−1.00...
E route	8.721...	−4.35...	$\left(\lambda_1, \frac{1}{\lambda_1}, \lambda_1, \frac{1}{\lambda_1}\right)$	−2.54...

values of the special ("degenerate") paths, cf. Tables II and III.

For this 32-64 renormalization calculation, the results seem to be nearly independent of F and G (values chosen between -10 and 10).

V. SUMMARY

All the scaling behavior in period-doubling of 2D area-preserving maps is observed in our symmetric quadratic 4D map. From this, one might already infer that asymptotically (as the period goes to infinity) our 4D map uncouples into two 2D maps. Furthermore, we conclude the following.

1. Stable regions in the *parameter* plane bifurcate into two regions when the period doubles. All such stable regions form a bifurcation tree in the parameter plane.

2. There are only three types of bifurcation routes (L, U, E routes). All bifurcation paths (with one exception for each route) in all L (U, E) routes have a second Feigenbaum constant (the convergence rate of the parameters) δ_2 of 4.000... ($-2.000...$, $-4.404...$), which is equal to the "contraction rate" γ for the L (U, E) routes.

3. The exceptional bifurcation path in the L (U, E) route corresponds to a bifurcation point with $\theta=0$ ($2\pi/3$, π). The value of δ_2 for the exceptional L and U route is $-15.1...$, which is the same as that found earlier in a nonsymmetric 4D map, cf. Ref. 6. The δ_2 for the exceptional path in the E route does not exist because this path is along the P axis (i.e., $E_n \equiv 0$) in the parameter plane.

4. An eigenvalue-matching renormalization shows that all regular paths limit on the three exceptional paths, at the rates 4.00..., $-2.00...$, and $-4.35...$ for the L, U, and E routes, respectively. These rates are equal to the three δ_2 values for the regular paths, but not to the δ_2 values of the exceptional paths.

Note that we have not studied the "opposite-phase" orbits of our 4D symmetric volume-preserving map. A more complete renormalization study,[10] including the renormalization of the parameters F and G, will be published elsewhere. That renormalization has been extended to a class of nonsymmetric maps [i.e., Eq. (2.1) with $f \neq g$] which is much larger than the class of symmetric maps discussed here. Nevertheless, it produces the same δ_1 and δ_2 value as found here for the symmetric maps.

ACKNOWLEDGMENTS

We have greatly benefited from discussions with G. Schmidt. J.M. is indebted to J. Greene and R. Schult for very useful discussions. This work was partially supported by the U.S. Department of Energy under Contract No. DE-AC03-84ER40182. The Center for Studies of Nonlinear Dynamics is affiliated with the University of California, San Diego.

APPENDIX A

In this appendix we indicate how to explicitly calculate the boundaries of the regions of stability, in the PE plane, for the orbits of period 2 and 4.

Introducing new coordinates (s_1,d_1,s_2,d_2) defined by

$$\begin{aligned} s_1 &\equiv \tfrac{1}{2}(x+u)(1+EF+EG) , \\ d_1 &\equiv \tfrac{1}{2}(x-u)(1+EF+EG) , \\ s_2 &\equiv \tfrac{1}{2}(y+v)(1+EF+EG) , \\ d_2 &\equiv \tfrac{1}{2}(y-v)(1+EF+EG) , \end{aligned} \tag{A1}$$

our map (2.1) becomes

$$\begin{aligned} s_1' &= -s_2 + f_1(s_1,d_1) , \\ s_2' &= s_1 , \\ d_1' &= -d_2 + f_2(s_1,d_1) , \\ d_2' &= d_1 , \end{aligned} \tag{A2}$$

where

$$\begin{aligned} f_1(s_1,d_1) &\equiv 2(Ps_1 + s_1^2 + \mu d_1^2) , \\ f_2(s_1,d_1) &\equiv 2[(P-2E)d_1 + 2\rho s_1 d_1] , \end{aligned} \tag{A3}$$

with

$$\begin{aligned} P &\equiv C+E, \quad \mu \equiv \frac{1+EF-EG}{1+EF+EG} , \\ \rho &\equiv 1-EH, \quad H \equiv \frac{2F+G}{1+EF+EG} , \end{aligned} \tag{A4}$$

The in-phase orbits of our map (2.1) become orbits of the new map (A2) with $d_1=d_2=0$. The Jacobian matrix of the map (A2) at the in-phase orbit is

$$\begin{aligned} \underline{J} &= \begin{bmatrix} 2P+4s_1 & -1 & 0 & 0 \\ 1 & 0 & 0 & 0 \\ 0 & 0 & 2(P-2E)+4\rho s_1 & -1 \\ 0 & 0 & 1 & 0 \end{bmatrix} \\ &\equiv \begin{bmatrix} \underline{J}_1 & 0 \\ 0 & \underline{J}_2 \end{bmatrix} , \end{aligned} \tag{A5}$$

where $\underline{J}_1$ and $\underline{J}_2$ are 2×2 matrices. The matrix $\underline{J}_1$ is the same as the one for period doubling in 2D area-preserving maps, cf. Eqs. (A2) and (A3), with $d_1=d_2=0$. The two invariants of the Jacobian matrix $\underline{J}$ of Eq. (2.6) can now be expressed as

$$\begin{aligned} T_1 &= \mathrm{Tr}\underline{J}_1 + \mathrm{Tr}\underline{J}_2 , \\ T_2 &= (\mathrm{Tr}\underline{J}_1)(\mathrm{Tr}\underline{J}_2) + 2 . \end{aligned} \tag{A6}$$

Hence the equations for, respectively, the PDB curve, TB curve, and CB curve (the three boundaries of the stable region) are

$$\mathrm{Tr}\underline{J}_1 = -2 \text{ or } \mathrm{Tr}\underline{J}_2 = -2 \text{ (PDB)} , \tag{A7}$$

$$\mathrm{Tr}\underline{J}_1 = 2 \text{ or } \mathrm{Tr}\underline{J}_2 = 2 \text{ (TB)} , \tag{A8}$$

$$\mathrm{Tr}\underline{J}_1 = \mathrm{Tr}\underline{J}_2 \text{ (CB)} . \tag{A9}$$

Substituting the coordinates of the period-2 orbit (cf. Appendix B), we find

$$\begin{aligned} \mathrm{Tr}\underline{J}_1 &= -2(P^2-4P-7) , \\ \mathrm{Tr}\underline{J}_2 &= \mathrm{Tr}\underline{J}_1 + 8E[2+2E+\Phi(P,E)] , \end{aligned} \tag{A10}$$

where

$$\Phi(P,E)\equiv H(P+1)(P-2E-4+2H)\ . \tag{A11}$$

Substituting Eqs. (A10) and (A11) into Eqs. (A7)–(A9), one obtains explicit expressions for those three boundaries of the stable regions of the period-2 orbits.

Explicit expressions for the three boundaries of the period-4 stable regions can also be given. The traces of $\underline{J}_1$ and $\underline{J}_2$ for the period-4 orbits are

$$\begin{aligned}
&\mathrm{Tr}\underline{J}_1=-16D(D-2\sqrt{D})+2\ ,\\
&\mathrm{Tr}\underline{J}_2=16[2E-EHP+(1-EH)\sqrt{D}\,]^2[P^2(1-2EH)-4E^2(1-HP)-2(1-EH)^2(P+\sqrt{D}\,)]\\
&\qquad +4E[2E-EHP-(1-EH)\sqrt{D}\,](2-HP)\ ,
\end{aligned} \tag{A12}$$

where $D\equiv P(P-2)$. Substituting Eq. (A12) into Eqs. (A7)–(A9) gives explicit equations for the three boundaries of the period-4 stable regions.

APPENDIX B

The coordinates x and y (or u and v) of the in-phase orbits satisfy Eq. (2.1). Hence they can be solved from

$$x'=-y+2[(C+E)x+(1+EF+EG)x^2],\quad y'=x\ . \tag{B1}$$

The coordinate transformation

$$X\equiv(1+EF+EG)x,\quad Y\equiv(1+EF+EG)y\ , \tag{B2}$$

puts the map (B1) in the standard form[12]

$$X'=-Y+2(PX+X^2),\quad Y'=X \tag{B3}$$

where

$$P\equiv C+E\ . \tag{B4}$$

That is, a bifurcation point on the P axis for the 2D map (B3) becomes a period-doubling bifurcation line (B4) in the PE-parameter plane for the 4D map (2.1).

We now show that $E=0$ is a CB curve on the PE plane: for $E=0$ the 4D map (2.1) uncouples into two 2D maps, and the eigenvalues of Jacobian matrix of the map are $(e^{i\phi},e^{-i\phi},e^{i\phi},e^{-i\phi})$. The invariants of its Jacobian matrix are

$$T_1=-4\cos\phi,\quad T_2=2(1+2\cos^2\phi)\ . \tag{B5}$$

Therefore we have

$$T_2=\frac{T_1^2}{4}+2\ , \tag{B6}$$

which is indeed the CB curve of Fig. 2, cf. Sec. II.

[1] *Universality in Chaos*, edited by P. Cvitanovic (Hilger, Bristol, 1983).

[2] R. Broucke, AIAA J. **7**, 6 (1969).

[3] P. Bak, T. Janssèn, and J. A. Tjon, Phys. Lett. **87A**, 139 (1982).

[4] R. S. MacKay, PhD. dissertation, Princeton University, 1982.

[5] T. Janssen and J. A. Tjon, J. Phys. A **16**, 673 (1983); **16**, 697 (1983).

[6] J. M. Mao, I. Satija, and B. Hu, Phys. Rev. A **32**, 1927 (1985).

[7] J. M. Mao, I. Satija, and B. Hu, Phys. Rev. A **34**, 4325 (1986).

[8] V. I. Arnold, *Mathematical Methods of Classical Mechanics* (Springer-Verlag, New York, 1979).

[9] J. Greene, R. S. MacKay, F. Vivaldi, and M. J. Feigenbaum, Physica **3D**, 468 (1981).

[10] J. M. Mao and J. Greene, La Jolla Institute Report, 1986 (unpublished).

[11] I. Walker and R. Kapral, Phys. Rev. A **30**, 2047 (1984).

[12] R. H. G. Helleman, in *Long-Time Prediction in Dynamics*, edited by W. Horton, L. Reichl, and V. Szebehely (Wiley, New York, 1982), pp. 95–126.

[13] B. Derrida, A. Gervois, and Y. Pomeau, Ann. Inst. Henri Poincaré **29**, 305 (1978); J. Phys. A **12**, 269 (1979).

[14] B. Hu and J. M. Mao, Phys. Lett. **108A**, 305 (1985).